Far-Field Boundary Conditions for Transonic Lifting Solutions to the Euler Equations

James L. Thomas* and M. D. Salas†
NASA Langley Research Center, Hampton, Virginia

Far-field boundary conditions for the Euler equations are formulated and applied to transonic lifting flow over an airfoil in an unbounded domain. An expansion of the linearized small-disturbance equation in the far field is developed and the leading-order term, corresponding to a point vortex representation for the airfoil, is retained. A comprehensive evaluation across the Mach number range of the procedure's effectiveness in eliminating dependence of the numerical results on the boundary extent is presented. Extension of the method to three dimensions is also outlined.

Introduction

THE flowfield disturbances generated by a lifting airfoil at subsonic or transonic freestream Mach numbers extend outward to large distances from the airfoil. A common practice in numerical solutions of the Euler equations for airfoil flows is to construct a body-fitted grid which extends sufficiently far from the airfoil so that the assumption of uniform freestream conditions on the outer boundary introduces negligible errors in the resulting solution. Thus, the boundary needs to extend quite far from the airfoil (> 50 chords) for accurate results. Such length scales are disparate with the small grid dimensions required near the airfoil to resolve the solution. The disparities can be overcome by either using a large number of grid points, which leads to long execution times, or using extreme grid stretching, which leads to cells of high aspect ratio and correspondingly lower accuracy. Alternatively, by matching the inner solution to a solution of a simpler far-field model equation the boundary extent can be reduced, leading to improvements in both accuracy and efficiency. Such a domain decomposition approach is developed below, matching a solution of the Euler equations in the interior to a solution of the linearized small-disturbance equation in the far field. In many cases, as discussed below, accurate computations can be made on grids extending on the order of five chords from the airfoil. As the Mach number is increased, however, regions of locally supersonic flow can extend quite far from the airfoil which, in turn, dictates a larger computational domain.

The idea of using a domain decomposition approach is certainly not new in computational fluid dynamics. For example, some form of asymptotic far-field boundary condition is used in all transonic potential methods applied to airfoils in unbounded flow. Most current methods use the leading-order term from the linearized small-disturbance equation, although the early work of Murman and Cole[1] used an expansion of the nonlinear transonic small-disturbance equation. The far-field expansion of the nonlinear equation was extended to three dimensions by Klunker.[2]

The influence of the computational mesh, including boundary extent, was noted in the potential and Euler solutions presented at the 1981 GAMM Workshop[3] on transonic flow. The major finding of that workshop was the wide discrepancy between full-potential and Euler calculations. However, the workshop also found sizable differences between results from different solution methods for the Euler equations, which subsequently led to the formation of an AGARD working group dealing with computed solutions to the Euler equations. The purpose of the working group was similar to that of the GAMM Workshop: to define a series of airfoil flows and compare calculations submitted by various contributors. The final report of the AGARD working group is forthcoming but, during the course of the study, the far-field boundary extent was identified as a dominant factor in the comparison of results from different methods at fixed angle of attack and Mach number. It was partly as a result of the establishment of this working group that the present effort was initiated. Several of the computations presented below are at conditions similar to those defined by the AGARD working group.

The effectiveness of the far-field boundary condition in reducing the dependence of computations on boundary extent is systematically evaluated below. Evaluations are made for an NACA 0012 airfoil at a 1-deg angle of attack across the Mach number range $M_\infty = 0.63\text{-}0.95$. The multigrid Euler solution of Jameson and Baker[4] was used. Converged solutions on a sequence of grids were obtained so that conclusions regarding boundary extent could be drawn independently of the spatial discretization. Extension of the present method to three dimensions is also outlined.

Governing Equations and Solution Method

The governing equations are the time-dependent Euler equations in control-volume form

$$\frac{\mathrm{d}}{\mathrm{d}t}\iiint_V \rho\,\mathrm{d}V + \iint_S \rho(q\cdot n)\,\mathrm{d}S = 0 \qquad (1)$$

$$\frac{\mathrm{d}}{\mathrm{d}t}\iiint_V \rho q\,\mathrm{d}V + \iint_S [\rho q(q\cdot n) + pn]\,\mathrm{d}S = 0 \qquad (2)$$

$$\frac{\mathrm{d}}{\mathrm{d}t}\iiint_V \rho E\,\mathrm{d}V + \iint_S \rho H(q\cdot n)\,\mathrm{d}S = 0 \qquad (3)$$

expressing the conservation of mass, momentum, and energy in a cell volume V bounded by a surface S with outward orientation n. The conserved variables ρ, ρq, and ρE represent density, momentum, and total energy per unit volume, respectively. The total enthalpy is $H(H = E + p/\rho)$ and the

pressure p is related to the conserved variables through the equation of state for a perfect gas, $p = \rho(\gamma-1)[E - q^2/2]$, where γ is the ratio of specific heats.

The above equations were solved with the finite-volume multigrid method of Jameson and Baker,[4] corresponding to a conservative central-difference scheme of second-order accuracy on uniform grids. Present results were obtained using the six-stage Runge-Kutta time integration scheme with residual smoothing described in Ref. 4. Calculations were made on a sequence of three O-type meshes, generally with grid densities in the chordwise and radial directions corresponding to 64×16, 128×32, and 256×64 cells, respectively; the latter two are of sufficient density that an accurate extrapolation to infinite spatial density can be made. On coarser meshes, successively fewer multigrid cycles were used; for example, 2, 3, and 4 V cycles were used for the preceding mesh sequence. On a 256×64 mesh, a scalar version of the code required 2.5×10^{-4} s per grid point per cycle on the VPS 32 (Cyber 205) computer at NASA Langley; a vector version was four times faster.

The forces acting on the airfoil in the steady state can be evaluated from either the surface pressures or from a momentum-flux balance; the latter is shown below.

$$c_a = \frac{-2}{\rho_\infty q_\infty^2 c} \oint_S (\rho u (q \cdot n) + p n_x) \mathrm{d}S \qquad (4)$$

$$c_n = \frac{-2}{\rho_\infty q_\infty^2 c} \oint_S (\rho v (q \cdot n) + p n_y) \mathrm{d}S \qquad (5)$$

The above integration is along a closed O-ring contour S enclosing the airfoil with outward-facing normal components n_x and n_y; c_a and c_n are the force coefficients in the axial and normal directions. The forces are nondimensionalized by the freestream dynamic pressure and the chord c. The two approaches to determine the forces should be equivalent for a conservative method, and the momentum-flux integrals [Eqs. (4) and (5)] should be invariant to the location of the contour S. Even though the numerical method used in the present investigation is conservative, the numerical fluxes differ from the Euler fluxes through the addition of second and fourth difference terms added to stabilize the calculation procedure. The radial variation of the flux integrals [Eqs. (4) and (5)], along with similar integrals of mass and total enthalpy, provide useful checks on the accuracy of the calculation as, for example, in the study of Ref. 5.

Far-Field Model

The basic premise in the development of the boundary conditions considered here is that the flow in the far field can be represented by the linear small-disturbance (Prandtl-Glauert) equation

$$(1 - M_\infty^2)\phi_{xx} + \phi_{yy} = 0 \qquad (6)$$

where ϕ denotes the perturbation potential and x and y denote the distances along and normal to the freestream velocity, corresponding to a Mach number M_∞. The above equation can be reduced to an incompressible equation,

$$\phi'_{x'x'} + \phi'_{y'y'} = 0 \qquad (7)$$

by applying an affine transformation where

$$x' = x, \qquad y' = \beta y \qquad (8)$$

and $\beta^2 = 1 - M_\infty^2$. The perturbation velocities and potential are related by

$$u = u'/\beta^2, \qquad v = v'/\beta \qquad (9)$$

$$\phi = \phi'/\beta^2, \qquad \Gamma = \Gamma'/\beta^2 \qquad (10)$$

The perturbation velocities in the far field can be represented as a Laurent series about the origin

$$u' = \sum_{n=1}^{\infty} \frac{1}{(r')^n} [b_n' \cos(n\theta') + c_n' \sin(n\theta')] \qquad (11a)$$

$$v' = \sum_{n=1}^{\infty} \frac{1}{(r')^n} [b_n' \sin(n\theta') + c_n' \cos(n\theta')] \qquad (11b)$$

where r' and θ' are the radius and polar angle, respectively, in the transformed plane. The coefficients b_n' and c_n' can be determined directly through a far-field expansion to a thin chord-line representation for the airfoil

$$c_n' = \frac{1}{2\pi} \int_0^c \omega' x^{n-1} \mathrm{d}x, \qquad n = 1,\infty \qquad (12)$$

$$b_n' = \frac{1}{2\pi} \int_0^c \sigma' x^{n-1} \mathrm{d}x, \qquad n = 1,\infty \qquad (13)$$

where the vorticity ω and source strength σ are related to the loading and thickness distributions

$$\frac{\omega}{q_\infty} = -\frac{1}{2}(C_{p,\text{upper}} - C_{p,\text{lower}})$$

$$\frac{\sigma}{q_\infty} = \frac{\mathrm{d}(\tau/c)}{\mathrm{d}(x/c)}$$

and C_p is the pressure coefficient and τ the airfoil thickness.

The leading terms in the transformed plane, decaying as the inverse of the radial distance, correspond to a point vortex and source representation for the airfoil. For a closed body, the only nonzero coefficient for the leading term is related to the circulation Γ'.

$$c_1' = \Gamma'/2\pi, \qquad b_1' = 0$$

The other terms, which decrease faster than the inverse of the radial distance, are related to moments of loading and thickness and are neglected in the results presented below. The coefficient of the dipole term in the loading can be taken to be zero by centering the origin at the airfoil moment center; for all subsequent calculations, the origin was centered at the airfoil quarter-chord, which is approximately the moment center for subcritical flows.

The perturbation velocities in the physical plane due to the leading-order term in the expansion are

$$u = \frac{\Gamma}{2\pi} \frac{\beta y}{x^2 + \beta^2 y^2} \qquad (14a)$$

$$v = \frac{-\Gamma}{2\pi} \frac{\beta x}{x^2 + \beta^2 y^2} \qquad (14b)$$

where the scaling of the circulation is determined from the airfoil lift coefficient c_ℓ,

$$\frac{\Gamma}{q_\infty} = \frac{c_\ell c}{2} \qquad (15)$$

The preceding model applies strictly to compressible flows without shocks. However, it can be extended to supercritical flows by recognizing that *the lift* computed from momentum considerations on closed intervals surrounding the body is invariant with distance from the airfoil and, thus, the far-field circulation can be determined from the lift using Eq. (15).

For supercritical flows, *the circulation* computed along closed intervals surrounding the body is not similarly invariant, since vorticity is generated at the shock, but does asymptote to a constant in the far field, namely, to that value given by Eq. (15). A similar extension of the small-disturbance linear equation to Euler flows has been given by Usab,[11] wherein the circulation in the far field is determined from the lift. The basic idea is to account for the subcritical flow surrounding a pocket of supercritical flow.

An example of this behavior is shown in Fig. 1 for super-critical flow over an NACA 0012 airfoil. The figure shows the variation of lift determined by integrating the momentum-flux equations [Eqs. (4) and (5)] along differing integration contours, and the lift deduced from circulation using Eq. (15). The abscissa is actually linear in the computational index corresponding to the integration contour; the average radius corresponding to the integration contour has more physical relevance and is denoted along the abscissa. The sketch showing the location of the sonic line is nearly to scale. The vorticity generated at the dominant upper surface shock produces a circulation of sign similar to the overall circulation due to lift, and thus the circulation increases outward from the body. For subcritical flows, the circulation integral is invariant with distance from the body. Note that with the transonic potential approximation, the circulation is always invariant because vorticity effects at the shock are not taken into account.

An alternative to relating the far-field coefficient in Eqs. (11) to the loading and thickness distribution is to determine the coefficients by matching, in a least-squares sense, the inner solution to the far-field representation at some nominal distance from the outer boundary. This approach is similar to an approach used recently by Wubs et al.[6] in a study of grid-size reduction for the incompressible flow equations. They showed that a substantial increase in efficiency could be obtained by increasing the number of terms from one to five in the far-field expansion, thereby allowing the outer boundary to be taken closer to the airfoil.

A far-field expansion of the compressible nonlinear small-disturbance approximation leads to the same functional behavior in the far field as given by Eqs. (11),[1] albeit with different coefficients. The coefficients arising from the nonlinear expansion are generally found from an integration over the entire flowfield.[1,2] Determining a few terms in Eqs. (11) by matching the interior solution to the far field by least squares is expected to be less computational work than per-forming a flowfield integration and, hence, could lead to further improvements in efficiency in regions of highly nonlinear flow.

Equations (14) and (15), for the perturbation velocities due to lift, can be combined with the freestream velocity and rotated into a body-oriented coordinate system with the freestream at angle of attack, α, to obtain the total velocities U and V in the far field

$$U/q_\infty = \cos\alpha + F\sin\theta \qquad (16a)$$

$$V/q_\infty = \sin\alpha - F\cos\theta \qquad (16b)$$

where

$$F \equiv (c_\ell c/4\pi)(\beta/r)[1 - M_\infty^2 \sin^2(\theta - \alpha)]^{-1} \qquad (16c)$$

and r and θ are the radius and polar angle, respectively, in the physical plane. The polar angle is defined positive counterclockwise from the chord line downstream of the air-foil quarter-chord. By assuming that the total enthalpy is constant, the preceding equations can be used to determine a local speed of sound along the boundary. Thus the far-field behavior of the solution has been modeled in a manner consistent with the inner solution; the far-field behavior is used in the boundary condition treatment given below.

Characteristic Treatment at the Boundary

Using the boundary condition of flow tangency on the air-foil and Eqs. (1-3), the flux evaluation on the airfoil requires only surface pressure. The pressure is determined by ex-trapolation using the normal momentum equation evaluated at the body. The boundary condition at the outer boundary is developed below.

A local coordinate system $(\hat{x}, \hat{y})$ is constructed orthogonal to the outer boundary with $\hat{x}$ normal to and directed out-ward from the boundary. Assuming that derivatives along the boundary can be neglected, $\partial(\ )/\partial\hat{y}\to 0$, the following characteristic equations can be constructed:

$$\frac{ds}{dt} = 0 \qquad \text{along} \quad C^0: \quad \frac{d\hat{x}}{dt} = \bar{u} \qquad (17)$$

$$\frac{d\bar{v}}{dt} = 0 \qquad \text{along} \quad C^0: \quad \frac{d\hat{x}}{dt} = \bar{u} \qquad (18)$$

$$\frac{d\bar{u}}{dt} \pm \frac{1}{\rho a}\frac{dp}{dt} = 0 \qquad \text{along} \quad C^\pm: \quad \frac{d\hat{x}^\pm}{dt} = \bar{u} \pm a \qquad (19)$$

where s is the entropy, a the local speed of sound, and $\bar{u}$ and $\bar{v}$ the local velocities. The characteristic paths are sketched in Fig. 2. Assuming locally homentropic flow, the last two equations become

$$\frac{d}{dt}(R^\pm) = 0 \quad \text{along} \quad \frac{d\hat{x}^\pm}{dt} = \bar{u} \pm a \qquad (20)$$

where the Riemann variables are

$$R^\pm \equiv \bar{u} \pm (2a/\gamma - 1)$$

The equations are in a form very similar to one-dimensional unsteady flow, the only exception being that tangential velocity as well as entropy are convected along the particle path.
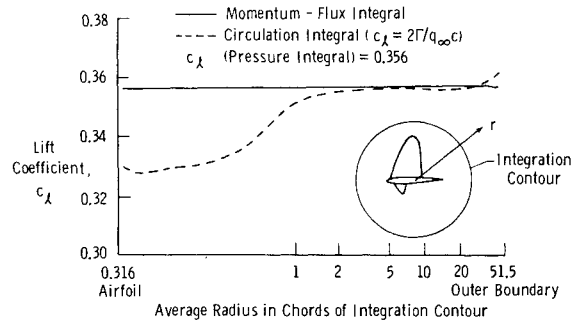

Fig. 1 Variation of lift deduced from momentum-flux and circula-tion integrations: $M_\infty = 0.80$; $\alpha = 1.25$ deg; 256×64 O-mesh.
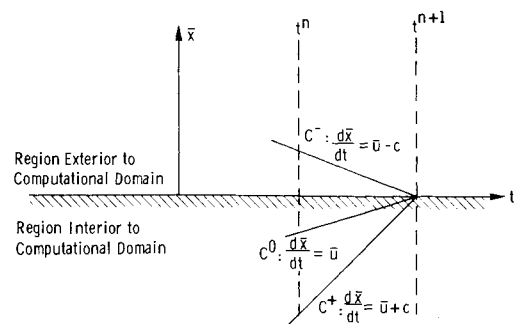

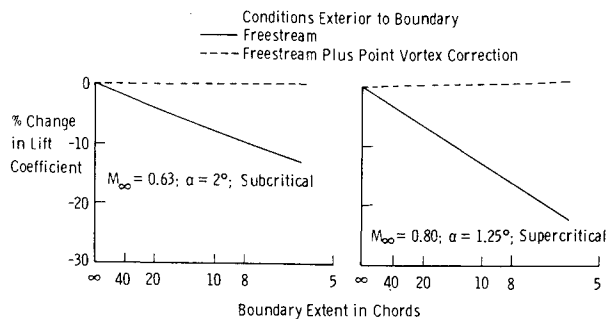Fig. 2 Sketch of characteristics at boundary with subsonic outflow $(\bar{u} > 0)$.

Fig. 3   Effect of boundary extent with fixed inner grid density: $192 \times (40\text{-}60)$ O-mesh.

a)   Residual history.

b)   Lift history.

Fig. 4   Effect of boundary extent with fixed grid density: $M_\infty = 0.8$; $\alpha = 1.25$ deg.

The characteristic equations are used to update the variables on the boundary at the new time level t^{n+1}, see Fig. 2. For subsonic conditions at the boundary, R^- can be evaluated locally from the far-field representation, Eqs. (16), corresponding to conditions outside the computational domain, and R^+ can be evaluated locally from the interior of the domain. The two Riemann variables can be added and subtracted to determine a local normal velocity and speed of sound at the boundary. Depending on the sign of the normal velocity (inflow or outflow), the entropy and tangential velocity $\bar{v}$ are extrapolated from the exterior or interior of the domain. Inflow corresponds to $\bar{u} < 0$ and outflow corresponds to $\bar{u} > 0$. In practice, the conditions exterior to the domain are evaluated at the cell interface location along the outer boundary, and the interior of the domain is taken to be the cell center adjacent to the boundary.

A shortcoming of the preceding procedure is that it does not guarantee the conservation of total enthalpy. Since the conservation of total enthalpy is an important feature of the numerical algorithm used in the interior point calculation, the speed of sound is redefined to ensure constant total enthalpy. As an alternative, one of the Riemann variables could be replaced by the specification of constant total enthalpy, or Eqs. (17-19) could be used without assuming locally constant entropy. Some numerical experiments using these ideas showed little effect on the computed results.

The above boundary conditions were first used in Ref. 7, and have since been used in a number of other works, including Ref. 4. The preceding discussion considered only the case of subsonic flow conditions on the far-field boundary. If the freestream is supersonic, the domain of dependence is considerably reduced and, consequently, the size of the computational domain can be reduced relative to that required for subsonic flow.

Computational Results

Several approaches were used to evaluate the dependence of the calculations on the boundary extent. The first is to decrease the extent of a given mesh by dropping grid lines from the outer boundary. This approach has the advantage of allowing the truncation error due to spatial discretization near the airfoil to remain the same. The second is to compute with a fixed grid density and variable outer boundary extent. By computing on a sequence of such meshes, an extrapolation can be made to eliminate the effects of spatial discretization from the effect of the outer boundary extent. The two approaches are illustrated below at two conditions for the NACA 0012 airfoil: 1) $M_\infty = 0.63$ and $\alpha = 2$ deg (subcritical), and 2) $M_\infty = 0.8$ and $\alpha = 1.25$ deg (supercritical).

Results from the first approach will be discussed subsequently. Initial results were obtained with an inverse radial stretching in the far field, which led to substantial numerical errors near the boundary due to excessive grid stretching. Subsequent results shown below were obtained by constraining the increase in radial lengths from one cell to another to be on the order of 1.2; several results with varying stretch
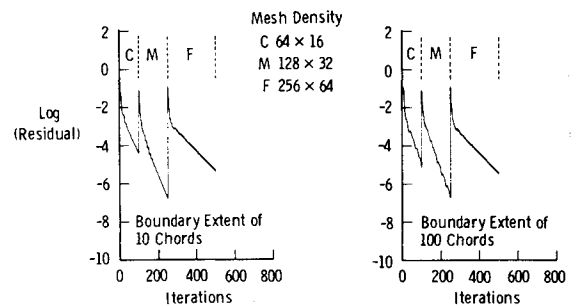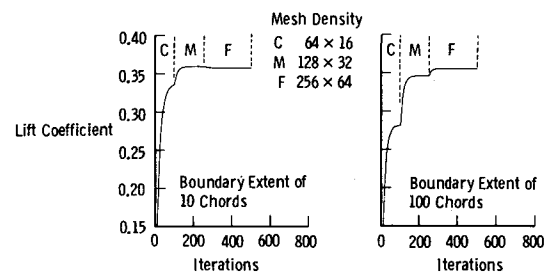
factors were obtained and the computations were insensitive in the range of radial stretching factors 1.1-1.3.

The precent change in section-lift coefficient as a function of varying grid extent is presented in Fig. 3. The grid used was an O-mesh with 192 cells around the airfoil and up to 60 cells outward from the airfoil. The boundary extent was reduced by eliminating grid cells outward from the airfoil. Using freestream conditions to update the far-field boundary conditions, the error in lift coefficient shows an inverse radial dependence on the boundary extent, which is the same functional behavior as the leading-order term in the far field. The supercritical case shows a stronger dependence on the outer boundary extent, as expected, due to the increased lateral extent of the disturbances at the higher Mach number. Updating the far-field boundary conditions using the far-field representation discussed previously leads to a solution with only a small dependence on the boundary extent and allows accurate computations with the boundary extent less than 10 chords. The subcritical lift ($c_\ell = 0.334$) compares very closely with a conservative full-potential code result. The supercritical case ($c_\ell = 0.358$) is beyond the limits of applicability of the conservative potential equations.[7]

These results are believed to be more accurate than those reported in the literature. For example, the computations of Ref. 8 on a grid extending 6 chords from the airfoil and using freestream conditions on the boundary are 6 and 14% lower than the present results for the subcritical and supercritical cases, respectively. Many of the computations in a recent workshop[9] are also considerably lower in comparison to the present results because freestream conditions were imposed in the far field.

Computations using the second approach are presented in Fig. 4. All of the computations given below, unless otherwise noted, are with the outer boundary updated using the point-vortex correction. The calculations were made with 100, 150, and 250 multigrid cycles (iterations) on the three meshes, respectively, and the residual history in Fig. 4a shows little effect of the boundary extent. For this supercritical case, the multigrid procedure is not as effective in reducing the residual on the finer meshes as on the coarser meshes. However, the lift history in Fig. 4b shows that the lift converges rapidly. The influence of the boundary extent is seen
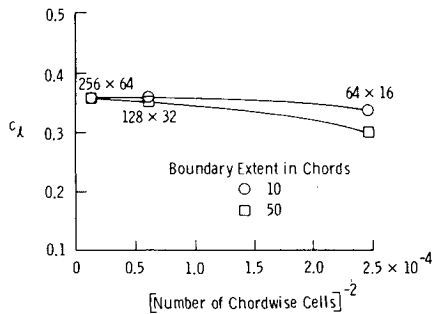
Fig. 5 Variation of lift with spatial density and boundary extent: $M_\infty = 0.80$; $\alpha = 1.25$ deg.
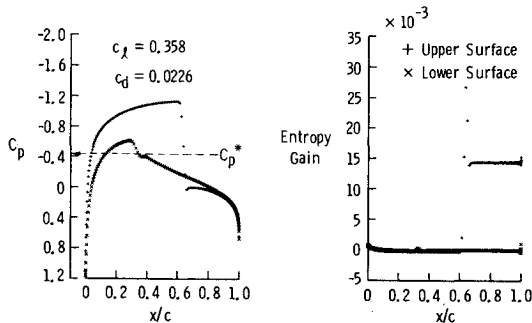

Fig. 6 Pressure and entropy distribution for supercritical case: $M_\infty = 0.8$; $\alpha = 1.25$ deg; 256×64 O-mesh.
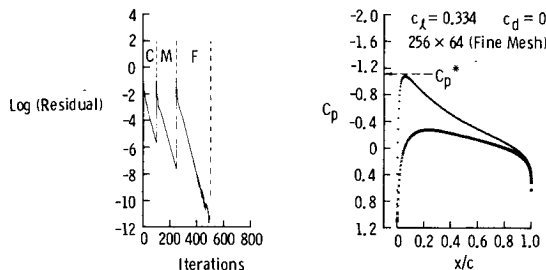

Fig. 7 Residual history and pressure distribution for subcritical case: $M_\infty = 0.63$; $\alpha = 2$ deg; 256×64 O-mesh.

Fig. 8 Lift variation with Mach numbers: NACA 0012; $\alpha = 1$ deg.
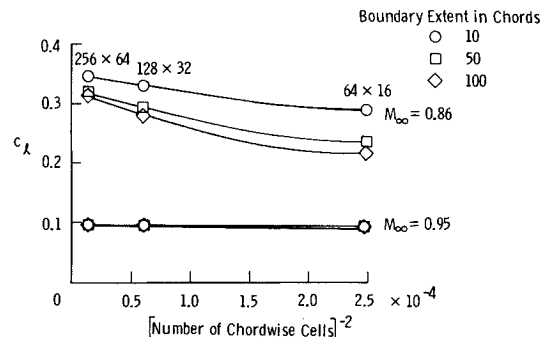
Fig. 9 Variation of lift with spatial density and boundary extent: $\alpha = 1$ deg.

in that, with the mesh extending 10 chords, an accurate computation is obtained on the medium-mesh density; with the mesh extending 100 chords, there is a substantial difference between the medium- and fine-mesh lift coefficients.

A similar effect is seen in Fig. 5, where the lift coefficient vs the inverse of the number of chordwise cells squared (for a second-order method, the variation of lift should be linear) is shown for two boundary extents. Results from the two boundary extents extrapolate to the same lift coefficient, although the spatial convergence is better with the smaller boundary extent, which corresponds to a finer discretization in the direction normal to the airfoil.

The pressure and entropy distributions for the supercritical case are shown in Fig. 6 with a boundary extent of 100 chords. The entropy gain is defined relative to the freestream entropy as

$$\left(\frac{p}{p_\infty}\right)\left(\frac{\rho_\infty}{\rho}\right)^\gamma - 1$$

and, as expected, it increases noticeably across the upper surface shock. The accuracy of the present calculations is evidenced in the very low level of entropy error in the leading-edge region. Corresponding residual and pressure distributions for the subcritical case are shown in Fig. 7 with
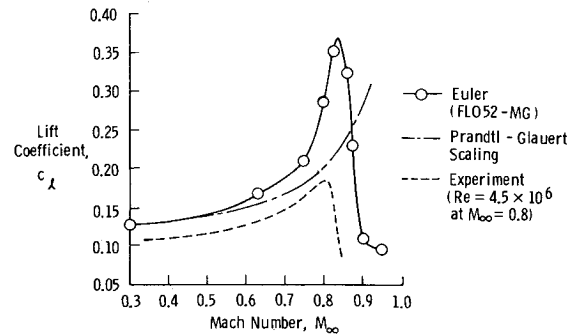
the boundary extent at 50 chords. The multigrid procedure is effective on all of the meshes. The drag coefficient on the fine mesh is less than half a count (<0.00005); although not shown, the absolute value of the entropy gain relative to freestream is less than 0.001 over the entire airfoil. The total pressure loss is proportional to entropy and total enthalpy losses raised to a power; for all cases presented here, the total enthalpy loss is on the order of machine zero.

Most of the effort in the present work has focused on the two cases presented above. Results similar to those above have been obtained with different mesh topologies and other integration schemes. For instance, the above procedure has been recently implemented into an implicit central difference scheme and demonstrated a similar insensitivity to boundary extent.[12] The present study was motivated, in part, by an attempt to compare the results of a recently developed upwind (flux-vector-splitting) code to results of other methods. With the improved boundary treatment, numerical comparisons of lift and drag from the upwind and central difference algorithms agree to within a few percent for both of the preceding cases.

The inviscid variation of lift with Mach number at a fixed angle of attack is shown in Fig. 8 for the NACA 0012 airfoil. For comparison, the linearized scaling and experimental values[10] at a nominal Reynolds number of 4.5 million are shown. The inviscid lift reaches a maximum near $M_\infty = 0.83$; the sharp decrease beyond that point is associated with the inefficient production of lift that occurs when the upper surface shock wave moves near the trailing edge.[10] The same phenomenon is evident in the experimental data, although the level of lift is lower than the inviscid values because of viscous effects. The linear theory predicts an infinite lift at $M_\infty = 1.0$ and departs from the Euler calculation past $M_\infty = 0.5$. Although not shown, results based on the conservative potential equation have been obtained and follow closely the Euler result below $M_\infty = 0.65$. Above $M_\infty = 0.65$, the values of lift obtained with the conservative potential equation are much higher than those obtained with the Euler equations.

The dependence of the computations on the boundary extent is presented below for two conditions in the highly nonlinear region beyond the maximum lift, $M_\infty = 0.86$ and 0.95. The variation of lift shown in Fig. 9 indicates that some sensitivity to the outer boundary extent occurs at $M_\infty = 0.86$, which is not entirely unexpected since the far-field-induced velocities in the present calculations do not account for the appreciable region of nonlinear flow. With a boundary extent of 10 chords, the lift is approximately 10% *higher* than on an infinite grid extent for $M_\infty = 0.86$. The variation of drag coefficient with boundary extent in Fig. 10 shows, in general, less variation than the lift but a similar increase in dependence on boundary extent at $M_\infty = 0.86$. Somewhat surprisingly, however, the results indicate considerably less influence of the boundary extent at $M_\infty = 0.95$; the lift and drag, as well as the pressure distribution on the airfoil, are nearly insensitive to the boundary extent.

For the preceding two cases, the radial variation of the circulation is shown in Fig. 11 and Mach number contours in Fig. 12. The vorticity generation and sonic lines extend much farther away from the airfoil for these cases than those shown previously; the sonic line at $M_\infty = 0.95$ extends laterally on the order of 20 chords. The lower surface shock is also much stronger for both of these cases and generates vorticity of opposite sign to that of the upper surface shock.
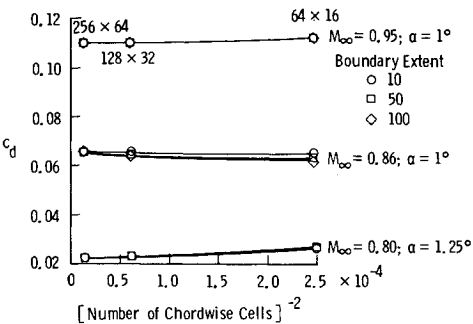

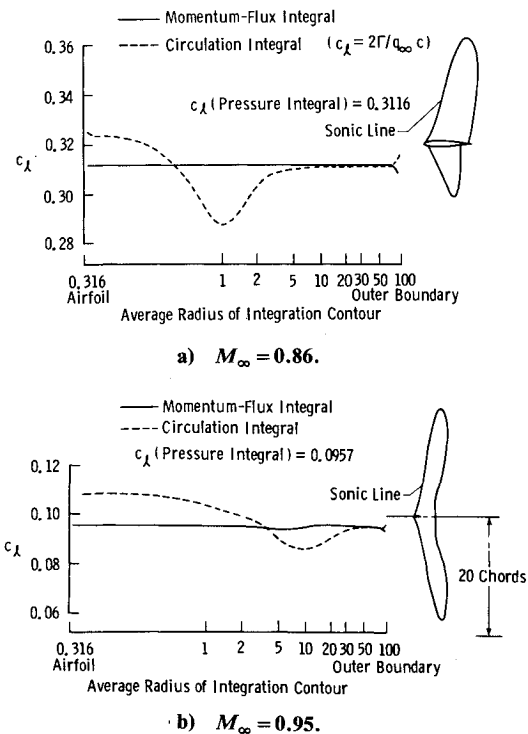Fig. 10   **Variation of drag coefficient with spatial density and boundary extent.**

a) $M_\infty = 0.86$.

b) $M_\infty = 0.95$.

Fig. 11   **Radial variation of circulation: $\alpha = 1$ deg; 256×64 O-mesh.**

The difference between the momentum-flux and circulation integrals at locations adjacent to the outer boundary (Fig. 11) is attributed to an incompatibility between the inner and outer solutions, since only the leading-order term in the far-field expansion is retained.

The reduced dependence of the lift and drag on the boundary extent at $M_\infty = 0.95$ in comparison to that at $M_\infty = 0.86$ is associated with the movement of both upper and lower surface shocks to the trailing edge, as evidenced in the oblique shock pattern shown in Fig. 12. At the higher Mach number, the airfoil is almost totally immersed in supersonic flow and consequently the domain of dependence is considerably reduced. The pressure distribution is predominantly influenced by the conditions along the inflow sonic line and only slightly by the shock waves downstream of the trailing edge. However, details of the flowfield outward from the airfoil are still sensitive to the boundary extent. For example, with grid extents of 10, 25, and 100 chords, the lateral extent of the sonic line was approximately 9, 16, and 19 chords, whereas the lift and drag changed less than a few percent. Hence, uniformly accurate results with the present approach are possible only if the outer boundary extends appreciably further than the extent of sonic flow.

Computations without the lift correction in the far field have been made for both of these cases. The results indicate a somewhat reduced sensitivity of lift to boundary extent at $M_\infty = 0.86$ (approximately 3% *loss* in lift with the boundary at 10 chords) and very little change at $M_\infty = 0.95$. It is expected that by increasing the number of terms in the far-field expansion, the dependency of the results to boundary extent at $M_\infty = 0.86$ could be reduced, since the sonic line extends only about two chords laterally.

Extensions to Three Dimensions

The method discussed herein can be extended to three dimensions in a straightforward manner. The characteristic treatment at the boundary is locally one-dimensional; additional work in three dimensions involves only the construction of a local coordinate system orthogonal to the boundary and the extrapolation of two tangential velocities instead of one.

The far-field representation in three dimensions has been develped by Klunker[2] and can be implemented in the present approach by replacing the point vortex model with a horseshoe vortex filament model in the transformed plane. As indicated by Klunker, the far-field contribution is dominated by terms associated with the lift. A single horseshoe vortex, whose magnitude scales on the total lift coefficient, could be used. Alternately, a series of filaments distributed across the span and scaling on the local lift coefficient could be used for a correspondingly more accurate definition in the far field. The effect of the boundary extent is lessened in three dimensions since the far-field-induced velocities diminish faster with radial distance than in two dimension, although the possible savings in computational work are substantially greater. It is expected that accurate results in three dimensions will require some representation of the induced velocities in the far field.
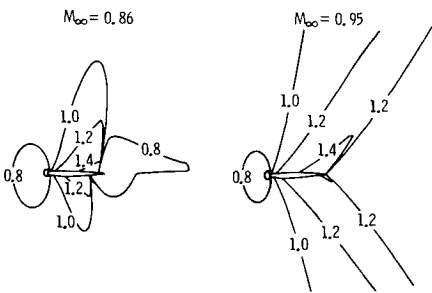

Fig. 12   **Mach contours: $\alpha = 1$ deg.**

Conclusions

Far-field boundary conditions for the Euler equations have been developed that incorporate the leading-order term in the asymptotic expansion valid at large distances from the airfoil. The formulation is easily implemented and the extension to three dimensions is straightforward. The effectiveness of the boundary conditions in reducing the dependence of the numerical results on the boundary extent has been evaluated systematically, including lifting solutions near Mach 1. The results indicate that accurate results can be obtained with a boundary extent of five chords for subcritical and mildly supercritical conditions. As the Mach number is increased, the lateral extent of the disturbances increases and larger extents are required for uniformly accurate results. However, once the upper and lower surface shocks move to the trailing edge, the forces and moments on the airfoil are generally insensitive to the boundary extent. It is expected that the present results could be further improved by including several more terms in the asymptotic expansion.

Acknowledgment

References

[1]Murman, E. M. and Cole, J. D., "Calculation of Plane Steady Transonic Flow," *AIAA Journal*, Vol. 9, Jan. 1971, pp. 114-121.

[2]Klunker, E. B., "Contribution to Methods for Calculating the Flow About Thin Lifting Wings at Transonic Speeds—Analytic Expressions for the Far-Field," NASA TN D-6530, 1971.

[3]Rizzi, A. and Viviand, H., eds., "Numerical Methods for the Computation of Inviscid Transonic Flows with Shock Waves: GAMM Workshop," *Notes on Numerical Fluid Mechanics*, Vieweg and Sohn, Wiesbaden, Germany, Vol. 3, 1981.

[4]Jameson, A. and Baker, T. J., "Multigrid Solution of the Euler Equations for Aircraft Configurations," AIAA Paper 84-0093, Jan. 1984.

[5]Yu, N. J., Chen, H. C., Samant, S. S., and Rubbert, P. E., "Inviscid Drag Calculations for Transonic Flows," Paper 83-1928, July 1983.

[6]Wubs, F. W., Boerstoel, J. W., and Van Der Wees, A. J., "Grid Size Reduction in Flow Calculations on Infinite Domains by Higher-Order Far-Field Asymptotics in Numerical Boundary Conditions," *Journal of Engineering Mathematics*, Vol. 18, 1984, pp. 157-177.

[7]Salas, M. D., Jameson, A., and Melnik, R. E., "A Comparative Study of the Non-Uniqueness Problem of the Potential Equation," NASA TP 2385, Jan. 1985.

[8]Pulliam, T. H., Jesperson, D. C., and Childs, R. E., "An Enhanced Version of an Implicit Code for the Euler Equations," AIAA Paper 83-0344, Jan. 1983.

[9]Reddy, K. C. and Steinhoff, J. S., "Computational Fluid Dynamics: A Workshop Held at the University of Tennessee Space Institute," UTSI E02-4005-023-84, March 1984.

[10]Mair, W. A. and Beaven, J. A., "Flow Past Airfoils and Cylinders," *Modern Developments in Fluid Dynamics—High Speed Flow*, Vol. II, edited by L. Howarth, Clarendon Press, Great Britain, 1953.

[11]Usab, W. J., Jr., "Embedded Mesh Solutions of the Euler Equations Using a Multiple-Grid Method," Ph.D. Dissertation, Massachusetts Institute of Technology, Cambridge, MA, 1983.

[12]Pulliam, T. H. and Barton, J. T., "Euler Computations of AGARD Working Group 07 Airfoil Test Cases," AIAA Paper 85-0018, Jan. 1985.